Revised Huang-Carter nonlocal kinetic energy functional for semiconductors and their surfaces

Xuecheng Shao [*], Wenhui Mi [†] and Michele Pavanello[‡]
Department of Physics, Rutgers University, Newark, New Jersey 07102, USA
and Department of Chemistry, Rutgers University, Newark, New Jersey 07102, USA

Nonlocal kinetic energy functionals with a density-dependent kernel are the most accurate functionals available for carrying out orbital-free density functional theory simulations. Among them, the Huang and Carter (HC) functional [Huang and Carter, Phys. Rev. B **81**, 045206 (2010)] is the most accurate for bulk semiconductors. A major hurdle in applying HC to nonbulk systems (such as clusters and surfaces which have at least one nonperiodic dimension where the density decays to zero) lies in its numerical instability for large values of the reduced density gradient, $s(\mathbf{r}) \propto \frac{|\nabla n(\mathbf{r})|}{n^{4/3}(\mathbf{r})}$, where n is the electron density. We propose a revision to the HC functional, revHC, that allows it to achieve dramatically improved numerical stability, efficiency (in terms of timing to solution), and applicability. Not only does revHC reproduce all previously presented results for HC, but it extends them to a crucially important class of materials: surfaces. We show that surface energy trends of clean-cut and reconstructed surfaces of group IV and III-V semiconductors are recovered and, where available semiquantitatively, reproduce the experimental results.

I. INTRODUCTION

The Kohn-Sham density functional theory (KS-DFT) [1,2] is the most widely used electronic structure method for systems that contain up to a few hundred atoms because it provides a good balance between accuracy and computational expense. However, KS-DFT requires the evaluation of the (noninteracting) kinetic energy T_s directly from the "one-electron" KS orbitals. Such a requirement leads to poor computational scaling [$O(N_e^3)$, where N_e is the number of electrons in the system] because of the computational cost involved in diagonalizing the Hamiltonian and overlap matrices. Therefore, systems with thousands or tens of thousands of atoms are either inaccessible or require specialized treatment [3,4]. Orbital-free DFT (OF-DFT) [5–7] and some formulations of DFT embedding [8–11] rely on pure density functionals of the noninteracting kinetic energy and are attractive alternatives for large-scale first-principles simulations because of their inherent linear-scaling computational cost. With these methods, simulations of simple metal bulks involving millions of atoms are possible [12,13], even with a single CPU [14]!

The underlying reason for such a computational advantage in OF-DFT is the use of kinetic energy density functionals (KEDFs), which are pure functionals of the electron density. For KS-DFT, even though the orbitals are formally functionals of the density, the kinetic energy is only indirectly a functional of the density through the KS orbitals. Thus, the accuracy of

orbital-free approaches is dominated by the accuracy of the employed KEDF [5,6].

Over many decades, several KEDFs have been proposed. They can be roughly categorized into two classes: (1) local/semilocal KEDFs [15–18] and (2) nonlocal KEDFs [19–30]. In local and semilocal KEDFs, the energy density and potential at point $\mathbf{r}$ depend exclusively on the density and its gradient at that same point (sometimes including high-order derivatives [31–34]). Semilocal KEDFs have the advantage of being evaluated with a low computational cost. Some semilocal KEDFs can approach results as good as nonlocal functionals for both metals and semiconductors [34,35]. However, semilocal KEDFs have inherent limitations such as the inability to describe the natural nonlocality of T_s and cannot reproduce the correct linear response behavior for uniform systems (the Lindhard response function) [36].

Nonlocal KEDFs overcome the issues above by encoding the correct physics in their kernel function $\omega[n](\mathbf{r}, \mathbf{r}')$, which describes the nonlocal kinetic energy as a six-dimensional integral from the dependence of the kernel on two distinct points in space, $\mathbf{r}$ and $\mathbf{r}'$. In principle, the kernel is related to the second functional derivative of the KEDF with respect to the electron density, and thus, it should be dependent on the electron density and should not be a simple function of $\mathbf{r}$ and $\mathbf{r}'$. The very first nonlocal KEDF with a density-dependent kernel was proposed and successfully adopted in real-materials simulations in 1985 [25]. However, its quadratic-scaling computational cost hindered this functional from being adopted for large-scale simulations. More recently, nonlocal KEDFs with density-dependent kernels have been proposed. To encode the required density dependence in the kernel, they employ either a Taylor expansion [24,27] around a reference constant density or spline techniques [28–30] to achieve a linear-scaling computational cost and applicability to metals

*xuecheng.shao@rutgers.edu
†wenhui.mi@rutgers.edu
‡m.pavanello@rutgers.edu

[24,27], semiconductors [28], and systems having inhomogeneous electron density such as quantum dots [29,30].

Unfortunately, as of today, there are no computationally efficient KEDFs which can work well for bulk systems as well as for nonperiodic systems, such as surfaces and clusters. Even one of the most sophisticated nonlocal functionals, the Huang-Carter (HC) KEDF [28], lacks the needed numerical stability to be able to approach nonbulk systems in a reliable and consistent way [37,38]. However, HC is perhaps the best functional because it satisfies many exact conditions for KEDFs. They include (1) recovering the linear response for a uniform electron gas, (2) approximately recovering the asymptotic behavior of a semiconductor's susceptibility function as the reciprocal space variable approaches zero [39], (3) uniform density scaling [40], and (4) the kernel being density dependent. Thus, efforts to improve HC's numerical stability and to enhance its applicability are well placed.

The source of the numerical instabilities in HC stems from the kernel function dependence on the term $k_F(\mathbf{r})s(\mathbf{r})^2|\mathbf{r} - \mathbf{r}'|$, with $s(\mathbf{r}) = \frac{|\nabla n(\mathbf{r})|}{2(3\pi^2)^{1/3}n(\mathbf{r})^{4/3}}$ and $k_F(\mathbf{r}) = [3\pi^2 n(\mathbf{r})]^{1/3}$. When systems have highly inhomogeneous electron densities, such as finite systems, the reduced gradient s can be very large, especially in the low electron density region. Because the gradient of the density is seldom accurate in the asymptotic region, the overall kernel becomes numerically unstable. Such instability increases the computational cost because the functional derivatives become numerically noisy.

In this work, we propose a revised HC functional (which we call revHC) such that it (1) satisfies all the exact conditions in the HC functional, (2) reproduces the HC functional results for bulk semiconductors, (3) is numerically stable for all kinds of systems, and (4) is computationally inexpensive or as inexpensive as nonlocal KEDFs with a density-*independent* kernel, such as Wang-Teter (WT) [19]. We achieve this by replacing the s^2 dependence with a Perdew-Burke-Ernzerhof (PBE) exchangelike enhancement factor (which is bound from above because it satisfies the Lieb-Oxford bound [41,42]) and by implementing revHC with the one-orbital ensemble self-consistent field (OE-SCF) density solver [43], dramatically reducing the computational cost.

With revHC, OF-DFT can now be employed in predictive simulations of semiconductor bulks and surfaces (clean and reconstructed) with an algorithm that scales favorably and (quasi)linearly with system size. In the following, we first discuss the formalism involved and then move to benchmark revHC on various semiconductor phases, comparing the results to the original HC functional as well as KS-DFT. We clearly show that revHC approaches semiconductor surfaces delivering semiquantitative results and reproducing the experimental trends.

II. THEORETICAL BACKGROUND

A. Huang-Carter KEDF

In this section, we summarize the main steps needed to derive and implement the HC KEDF. The HC total kinetic energy can be written as

$$T_s[n] = T_{\text{TF}}[n] + T_{\text{vW}}[n] + T_{NL}[n], \tag{1}$$

where $T_{\text{TF}}[n]$ and $T_{\text{vW}}[n]$ are the local Thomas-Fermi (TF) KEDF [15,16] and von Weizsäcker (vW) KEDF [44], respectively. And the nonlocal term can be written as

$$T_{NL}[n] = C_{\text{HC}} \iint \rho(\mathbf{r})^{8/3-\beta} \omega[\xi(\mathbf{r}, \mathbf{r}')|\mathbf{r} - \mathbf{r}'|]\rho(\mathbf{r}')^{\beta}. \tag{2}$$

β is a constant positive parameter. The kernel ω depends on the effective Fermi wave vector $\xi(\mathbf{r}, \mathbf{r}')$ and the distance $|\mathbf{r} - \mathbf{r}'|$. To recover the correct long-range asymptotic behavior of the susceptibility function [i.e., $\chi(|\mathbf{r} - \mathbf{r}'| \to \infty) \to |\mathbf{r} - \mathbf{r}'|$ or $\hat{\chi}(q \to 0) \to -bq^2$] for semiconductors, ω should tend to $1/|\mathbf{r} - \mathbf{r}'|$ when $|\mathbf{r} - \mathbf{r}'| \to \infty$. To approximately satisfy this requirement, the effective Fermi wave vector $\xi(\mathbf{r}, \mathbf{r}')$ can be chosen to have the following form:

$$\xi(\mathbf{r}, \mathbf{r}') = k_F(\mathbf{r}) \left\{ 1 + \lambda \left[\frac{\rho(\mathbf{r}) - \rho(\mathbf{r}')}{|\mathbf{r} - \mathbf{r}'|} \right]^2 \frac{1}{\rho(\mathbf{r})^{8/3}} \right\}. \tag{3}$$

Above, $k_F(\mathbf{r}) = [3\pi^2 \rho(\mathbf{r})]^{1/3}$ is the Fermi wave vector, and λ is used for tuning the contributions between the $|\mathbf{r}' - \mathbf{r}|$ term and the $1/|\mathbf{r}' - \mathbf{r}|$ term in the kernel. When $\lambda = 0$, the kernel will just satisfy the asymptotic behavior for metals.

Adopting directly the two-point density-dependent formalism of Eq. (3) will lead to a quadratic scaling computational cost. To reduce the computational complexity, $\xi(\mathbf{r}, \mathbf{r}')$ is further approximated by the single-point density-dependent form:

$$\xi_{\text{HC}}(\mathbf{r}) = k_F(\mathbf{r})[1 + \lambda c s(\mathbf{r})^2], \tag{4}$$

where s is the reduced gradient and the constant $c = [2(3\pi^2)^{1/3}]^2$.

To make sure uniform systems are still within the regime of applicability of the proposed functional and because of the simple explicit form provided by the Lindhard function, the kernel then is determined by enforcing the exact linear response of the uniform electron gas (Lindhard response) in the limit of uniform densities. Namely,

$$\hat{\mathcal{F}}\left(\frac{\delta^2 T_s[n]}{\delta n(\mathbf{r})\delta n(\mathbf{r}')} \bigg|_{n(\mathbf{r})=n_0} \right) = -\frac{1}{\tilde{\chi}_{\text{Lind}}(q)}, \tag{5}$$

where $\hat{\mathcal{F}}$ represents the Fourier transform operator, n_0 is the uniform electron gas density, and $\tilde{\chi}_{\text{Lind}}$ is the Lindhard response function,

$$\tilde{\chi}_{\text{Lind}}(\eta) = -\frac{k_F}{\pi^2}\left(\frac{1}{2} + \frac{1-\eta^2}{4\eta} \ln\left| \frac{1+\eta}{1-\eta} \right| \right) = -\frac{k_F}{\pi^2}\frac{1}{G(\eta)}, \tag{6}$$

where $\eta = q/2k_F$ is a dimensionless momentum vector and $k_F = (3\pi^2 n_0)^{1/3}$. We stress that the above equation in no way restricts the susceptibility of the system to be the Lindhard function because through Eq. (3), the effective response function for nonhomogeneous systems is different from the Lindhard function. Imposing of Eqs. (1) and (2) and using Eq. (4) in Eq. (5), a first-order ordinary differential equation for the kernel can be obtained:

$$-\beta\eta\tilde{\omega}(\eta)' + (5 - 3\beta)\beta\tilde{\omega}(\eta) = 5/3[G(\eta) - 3\eta^2 - 1]. \tag{7}$$

The kernel can be numerically solved with a given constant parameter β.

B. Revised HC KEDF

The success of HC in modeling semiconductors hinges on the correct asymptotic behavior of its kernel. Unfortunately, ξ_{HC} in Eq. (4) can lead to numerical instabilities and, as a result, convergence issues. When systems display strong inhomogeneous electron densities (such as isolated systems and surfaces), especially in the low electron density region, the numerical values of s^2 can be very large because of its inverse dependence on the electron density. When low density values are coupled with inaccurate density gradient values (as often happens in the asymptotic region), the ensuing numerical noise negatively affects convergence.

In addition, HC suffers from a deeper problem related to the estimation of the resulting integrals for the evaluation of energy density and potential. Similar to almost [36] all nonlocal functionals with a density-dependent kernel (KEDF [29] as well as exchange correlation [45,46]), integrals are apparently of quadratic cost (i.e., they feature a double integration over the fast Fourier transform grid). However, they can be approximated by a spline technique [47] in which the kernel is evaluated as a function of a constant×$|\mathbf{r} - \mathbf{r}'|$ sampling over the constant and then using splines and/or numerical Riemann integrals to recover the final result. If the kernel depends on only the density and not on its gradient [29], this technique delivers numerically stable energy densities and potentials. However, because in HC the kernel also depends on s^2 (which, as mentioned, can reach large values in nonperiodic systems), the splines often require wide sampling windows, increasing the computational costs significantly [38].

To overcome these limitations, we propose a revised HC functional which approximates ξ_{HC} as

$$\xi_{\text{revHC}}(\mathbf{r}) = k_F(\mathbf{r})F_{\text{revHC}}(s(\mathbf{r})), \qquad (8)$$

where $F_{\text{revHC}}(s)$ is an enhancement factor, similar to the one used in GGA functionals. To compare it to the original HC functional, the enhancement factor for HC would be $F_{\text{HC}}(s) = 1 + \lambda c s^2$, where $c = [2(3\pi^2)^{1/3}]^2$. We require $F_{\text{revHC}}(s)$ to have the following properties: (1) it should tend to $1 + \lambda c s^2$ for small s, (2) it should approach a finite asymptote for large s to avoid numerical noise and an increase in computational cost, and (3) it should be a smooth function. To satisfy these properties, we choose an enhancement factor similar to the one used in the exchange part of the PBE functional. Namely,

$$F_{\text{revHC}}(s) = 1 + \frac{as^2}{1 + bs^2}. \qquad (9)$$

When $b = 0$, revHC is the same as the original HC. $\lambda = 0.01$ was chosen for the original HC functional to model cubic diamond (CD) silicon—a value corresponding to $a = \lambda c \approx 0.38$ and $b = 0$. When given a nonzero b, $F_{\text{revHC}}(s)$ smoothly approaches a constant value for large s. Figure 1 compares the enhancement factors of HC with $\lambda = 0.01$ and revHC with $a = 0.45$ and $b = 0.10$. The values for the a and b parameters were obtained by fitting, imposed to reproduce the equilibrium volume and energy of CD Si. It is clear that F_{revHC} satisfies the requirements enumerated before. In Fig. 1, we also superimpose a green histogram of the distribution of points in space where the electron density for the Si (111) surface is below 10^{-3}. These are points where the gradient
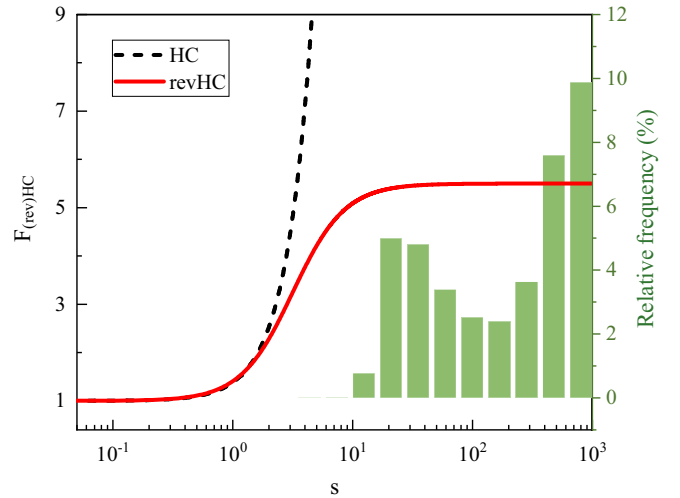

FIG. 1. Enhancement factors of the original HC KEDF with $\lambda = 0.01$ (dashed black line) compared to the one for the revHC KEDF with $a = 0.45$ and $b = 0.10$ (solid red line). The green histogram is the distribution of grid points with low electron density ($<10^{-3}$) plotted against the s value at those points for the Si(111) surface. Such points hardly exist in a bulk crystal.

starts becoming inaccurate and s^2 reaches unphysically large values. Because of the asymptote, F_{revHC} dampens the detrimental effect of these inaccurate s^2 values. In this work, we choose $a = 0.45$ and $b = 0.10$ for all calculations. In revHC, the constant parameter β is fixed to 2/3, which is close to the value of 0.65 chosen for the original HC functional for CD Si. We found that this value of β produces the best results and generates a kernel that is similar to that of other successful functionals [19,27].

Imposing the redefined ξ_{revHC} from Eqs. (8) and (9) on the functional formalism of Eq. (2), revHC's kinetic energy and its functional derivative (needed for solving for the electronic structure) are obtained. By enforcing the Lindhard response, the kernel equation is obtained in exactly the same way as the kernel of the original HC functional given in Eq. (7).

III. COMPUTATIONAL DETAILS

We use the same linear-scaling techniques as the original implementation of HC to evaluate the nonlocal energy density and potential. The details of such techniques can be found in the Appendix of Ref. [28]. Only a few minor changes have been implemented. When building the spline quadrature, we use a smaller ratio ($\kappa = \xi_{i+1}/\xi_i = 1.15$ and $\xi_1 = 0.01$) to better converge the total energy (typically, within 1 meV/atom). In the case that $\xi < \xi_1$ we opt for a linear interpolation.

HC and revHC are implemented in DFTPY [14], which is an open-source PYTHON code for large-scale OF-DFT simulations [48]. The KS-DFT calculations are performed with CASTEP [49]. All calculations use the bulk-derived local pseudopotentials (BLPS) [50], except for Germanium (Ge) for which we use the optimal effective local pseudopotential (OEPP) [51]. The local density approximation for the electron exchange-correlation functional is adopted throughout [52]. The kinetic energy cutoff for the density is chosen to be

1600 eV, except for the surface energy calculations, where it was increased to 3200 eV. For the benchmark KS-DFT calculations, a 1200 eV cutoff for the kinetic energy of the wave functions is chosen, and a $20 \times 20 \times 20$ k-point mesh is used for bulk system calculations to obtain well-converged total energies (1 meV/atom). CD, hexagonal diamond (HD), and complex bcc (cbcc) are selected as three silicon semiconductor phases. Nine III-V cubic zinc-blende (ZB) semiconductors also are selected as benchmark systems. The bulk modulus, equilibrium volumes, and equilibrium energies were calculated by expanding and compressing the KS-DFT equilibrium unit cell structure up to 5% with 11 points and fit the energy curves vs volume against Murnaghan's equation of state [53]. In OF-DFT, the OE-SCF solver [43] was adopted for all density optimizations.

For the unreconstructed surface energy calculations, the unreconstructed surfaces are modeled by at least 10 layers with 15 Å vacuum between periodic slabs. The reconstructed surfaces were relaxed using analytic forces and energies from the in-house code EDFTPY through an application programming interface (API) to Atomic Simulation Environment (ASE) [54]. ASE contains a set of tools and PYTHON modules for atomistic simulations, including geometry relaxations. We refer the reader to Ref. [43] for details regarding the implementation of the OE-SCF density optimization method. The surface structures were created with experimental lattice parameters [55]. The surface energy is evaluated by

$$\sigma = \frac{E_{\text{slab}} - N E_{\text{bulk}}}{2 A_{\text{slab}}}, \quad (10)$$

where E_{slab} is the total energy of the slab model, E_{bulk} is the energy per atom of the bulk structure, N is the total number of atoms in the slab, and A_{slab} is the surface area of the slab.

IV. RESULTS AND DISCUSSION

A. Bulk properties of semiconductors

The HC functional was designed to accurately predict various group IV and III-V semiconductors. Therefore, we wish revHC to be as accurate as HC for these systems. To benchmark the quality of the revHC functional, we compute the total energy versus volume equation of states for CD silicon with KS-DFT and OF-DFT with the HC, revHC, and Wang-Govind-Carter 1999 (WGC99) [27] functionals using the same pseudopotentials (BLPS). As shown in Fig. 2, the curve obtained by KS-DFT is well reproduced by the HC and revHC functionals. revHC is almost on top of KS-DFT, whereas WGC99 overestimates the energy by a few hundred meV.

We also find revHC to be as transferable as HC. In Table I, we list the bulk properties of three silicon semiconductor phases calculated with revHC in comparison with KS-DFT as well as the original HC results. revHC results are very close to HC's, and both are in good agreement with KS-DFT.

Vacancy and interstitial formation energies as well as phase energy ordering are considered tough yet important tests for the accuracy of a KEDF. The original HC, for example, could semiquantitatively reproduce the vacancy formation energy but failed for the interstitial formation energy. Provided that the parameter λ is optimized, HC could reproduce phase
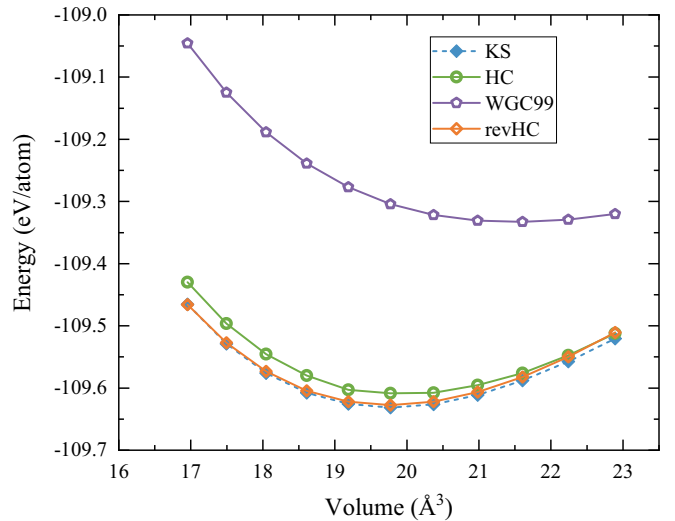

FIG. 2. KS-DFT and OF-DFT total energy curves versus volume for bulk CD silicon. HC and WGC99 results were calculated using PROFESS 3.0 [56]. The WGC99 parameter γ was set to 4.2 [57], which is the default for this phase of silicon.

energy orderings [except for the body-centered-tetragonal 5 (BCT5) phase]. revHC is expected to behave similarly to the HC functional in these cases. In fact, we find that the vacancy formation energy is only slightly improved compared to HC. The interstitial formation energy is essentially unchanged from HC, predicting it with the wrong sign (see Table S2 in the Supplemental Material [58]; we refer the reader to Ref. [28] for details about this failure of HC). Phase energies are well reproduced by revHC provided that the a parameter is adjusted in a way that is analogical to the λ parameter of HC (see line revHC^a in Supplemental Material [58], Table S3).

In a second test, we use revHC to test III-V ZB semiconductors. The energy differences between CD silicon and III-V ZB semiconductors are presented in Fig. 3. revHC and HC are on top of each other and reproduce well the KS-DFT results. These results indicate that revHC is as predictive as the HC functional in terms of both accuracy and transferability when

TABLE I. Bulk modulus B_0 and equilibrium volume V_0 of silicon in CD, HD, and cbcc phases obtained by KS-DFT, HC, and revHC. The equilibrium energy for CD silicon and the energies of other two structures relative to the CD phase are presented. The HC values are taken from Ref. [28].

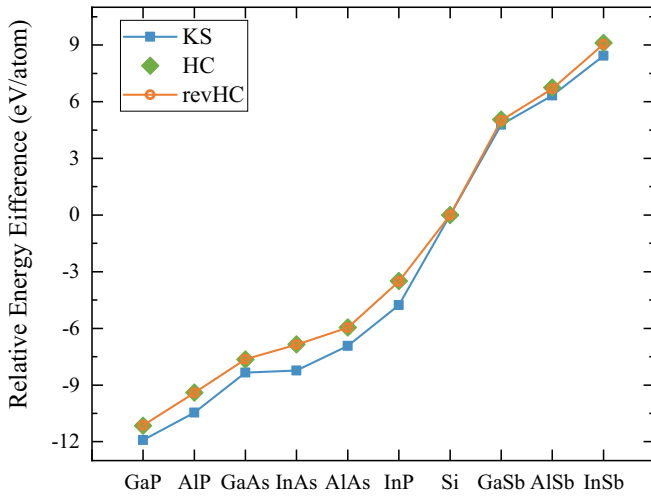| Si	Functional	B_0 (GPa)	V_0 (Å³/atom)	E_0 (eV/atom)
CD	KS	96	19.779	−109.631
	revHC	98	19.765	−109.627
	HC [28]	97	19.962	−109.624
HD	KS	97	19.643	0.014
	revHC	99	19.738	0.004
	HC [28]	98	19.875	0.007
cbcc	KS	99	17.520	0.156
	revHC	99	18.198	0.122
	HC [28]	105	18.419	0.141

FIG. 3. OF-DFT and KS-DFT relative energy differences between CD silicon and ZB semiconductors. The HC values are taken from Ref. [28]. Note that the revHC values are on top of HC's.

modeling semiconductors (see Table S1 for a complete set of results).

B. Semiconductor surfaces

To our knowledge only the Si (100) surface has been computed by the HC functional [38]. The reason is probably because the HC functional is slowly convergent for systems with highly inhomogeneous density, such as surfaces and clusters. The reported surface energy values are $\sigma = 0.152 \, \mathrm{eV/\mathring{A}^2}$ for Si (100) unreconstructed and $\sigma = 0.119 \, \mathrm{eV/\mathring{A}^2}$ for the reconstructed surface. These values overestimate the KS results by 7% and 59% for unreconstructed and reconstructed surfaces, respectively [38].

Because the revHC functional resolves problems of convergence and computational complexity when associated with the OE-SCF solver [43], in this work we are able not only easily compute surface energies for all the semiconductors considered so far, but we also could optimize the geometries of the slabs involved with the revHC functional, reducing significantly the discrepancy against the experiment and the KS-DFT surface energy values.

In Tables II and III, we show that for group IV and III-V semiconductor surfaces derived by cleanly cutting the bulk (unreconstructed), the revHC functional performs well with surface energy deviations between +24% and −5% with values almost always overestimated compared to KS. The overall assessment for revHC is, however, positive because the surface energy ordering for Si and Ge is recovered, and it is essentially recovered also for the III-V semiconductors. This shows that revHC not only is predictive for bulk phase ordering and equations of state but retains such a predictivity also for semiconductor surfaces.

We tested revHC for its ability to reproduce the surface energy of simple metals, such as aluminum. We find that the surface energies of (111), (110), and (100) facets are reproduced with deviations ranging from −11% to 4% compared against KS-DFT. This accuracy is similar to that for semiconductor surfaces (see Supplemental Material [58], Table

TABLE II. Comparison of various surface energy values of Si and Ge calculated with revHC compared against experimental values. The KS and KS(US) results were calculated by CASTEP with the same local pseudopotentials as the OF-DFT simulations and the GBRV ultrasoft pseudopotentials [59], respectively. RE is the relative error of revHC compared to KS.

System	Surface	Surface energy (eV/Å²)			RE
		revHC	KS	KS(US)	
Si	(111)	0.092	0.097	0.113	−5%
	(110)	0.120	0.111	0.127	8%
	(100)	0.159	0.128	0.148	24%
Ge	(111)	0.079	0.078	0.083	1%
	(110)	0.110	0.091	0.096	21%
	(100)	0.114	0.105	0.108	9%

S4). An important test, however, is to confirm revHC's good behavior also for reconstructed surfaces. They are very different from the clean bulk-cut surfaces because they feature complex patterns whose geometries depart sharply from the atomic arrangement of the corresponding bulk. In Table IV we present results of surface energies for reconstructed Si surfaces computed with revHC as well as KS (with BLPS as well as ultrasoft pseudopotentials). Table IV also includes results of the revHC functional where the surfaces have been relaxed to the optimal structure for this functional. As expected, the surface energies are overestimated for the revHC unrelaxed surfaces, while for the relaxed surfaces (i.e., the revHC column in Table IV) revHC's surface energies are much closer to the experimental values.

An important observation is that the revHC optimized surfaces are not drastically different from the KS-DFT optimized surfaces. In Fig. 4, we show the main differences between the optimized revHC and KS-DFT Si (111) reconstructed surfaces (Figs. S1 and S2 in the Supplemental Material [58] show the other two surface cuts). The biggest differences between the two surfaces are highlighted in Fig. 4 and involve the shortening of two bonds (the biggest bond contraction is by about 20%, occurring in the bond at the top of the slab in Fig. 4). This is in line with the general observation that HC and other nonlocal KEDFs with a density-dependent kernel tend to overestimate the atomic average coordination number.

TABLE III. Surface energies of the (110) cut of several III-V semiconductors. See Table II for additional information.

System	Surface energy (eV/Å²)			RE
	revHC	KS	KS(US)	
AlP	0.115	0.118	0.100	−3%
AlAs	0.103	0.105	0.087	−2%
AlSb	0.083	0.079	0.069	5%
GaP	0.122	0.114	0.096	7%
GaAs	0.107	0.100	0.081	7%
GaSb	0.089	0.077	0.065	17%
InP	0.096	0.100	0.075	−4%
InAs	0.087	0.090	0.065	−3%
InSb	0.080	0.071	0.054	12%

TABLE IV. Surface energy values of reconstructed surfaces of silicon. Structures are taken from Ref. [60]. The KS(PAW) values are taken from the same reference and are computed with PAW pseudopotentials. See Table II for additional information.

System	Surface	Surface energy (eV/Å^2)					
		revHC[a]	revHC	KS	KS(US)	KS(PAW) [60]	Experiment
Si	(111)	0.082	0.111	0.081	0.092	0.081	0.077 [61], 0.077 [62], 0.071 [63]
	(110)	0.126	0.128	0.087	0.105	0.094	0.094 [61], 0.089 [62], 0.119 [63]
	(100)	0.078	0.116	0.075	0.091	0.080	0.133 [61], 0.085 [62]

[a]Surfaces relaxed by OF-DFT with the revHC functional.

C. Computational cost

To evaluate the computational efficiency of the revHC KEDF, we compare the total wall time and number of density optimization steps for different CD Si cubic supercells. For comparison, data from the density-independent-kernel KEDF, WT [19], are also presented. We adopted the OE-SCF [43] OF-DFT solver. From the timings reported in Fig. 5, it is clear that revHC retains quasilinear scaling cost with system size. revHC's timings are even comparable with WT's. Given that WT is the least computationally expensive nonlocal KEDF, we conclude that the revHC functional combined with the OE-SCF solver can be used for predictive large-scale simulations, just like WT has been [12–14,64]. The OE-SCF solver requires only the evaluation of the nonlocal part of revHC a handful of times (as many times as the number of cycles needed to converge). The use of OE-SCF coupled with the inherent more robust numerical behavior of revHC compared to HC is the reason why our implementation of revHC is much more computationally efficient than previous implementations of HC. In our view, this is an important improvement of the current state of the art.

V. CONCLUSIONS

Despite the fact that HC is one of the most accurate kinetic energy functionals available (certainly, the most accurate for semiconductors), numerical inaccuracies prevent its applica-

tion to a wide class of systems, i.e., nonperiodic systems in which the density decays to zero along one or more dimensions. Beyond the purely numerical challenges, the high computational cost has relegated this functional to the computation of only small toy systems.

In this work, we tackled both the numerical and computational complexity challenges by proposing a revised version of HC: revHC. We found revHC to be as accurate as HC for the systems where HC was found to be excellent (semiconductor bulk systems). At the same time, revHC extends HC's applicability to nonperiodic systems, such as surfaces.

We found revHC to deliver quantitative results for the equilibrium volumes, bulk moduli, and phase energy ordering for Si and other semiconductors. In addition, the surface energies of Si, Ge, and nine III-V semiconductors compared semiquantitatively against KS-DFT. The surface energies of the reconstructed surfaces of Si were found to be in excellent agreement with the experiment provided that the computed slabs are relaxed. From the point of view of the computational complexity, when the OE-SCF solver is used [43], revHC is found to be only slightly more expensive than the computationally cheapest of the nonlocal functionals (the WT [19] functional). Overall, our results indicate that revHC should become the kinetic energy functional of choice for large-scale orbital-free DFT simulations involving semiconductor materials.
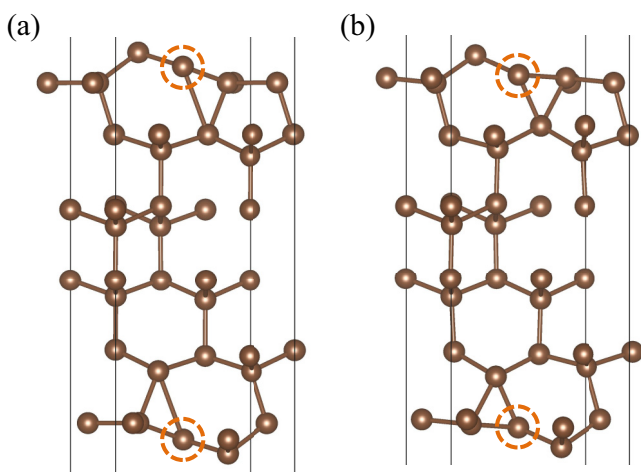

FIG. 4. Optimized (relaxed) reconstructed Si (111) surfaces computed by (a) KS-DFT and (b) revHC. The highlighted atoms are the ones displaying the largest geometrical rearrangement.
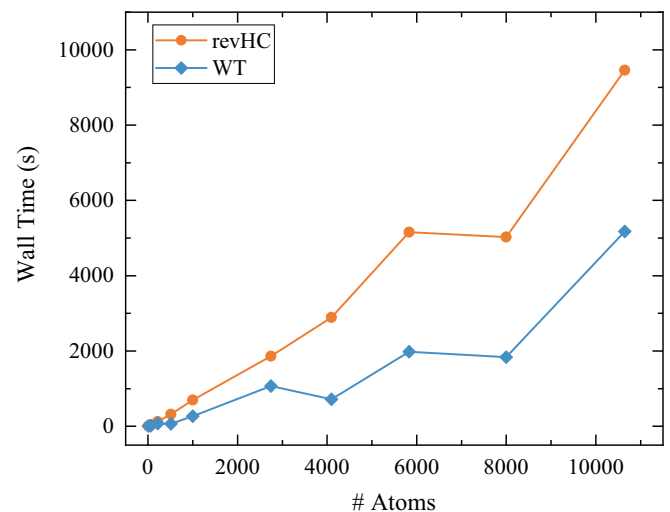

FIG. 5. Wall times of single-point OF-DFT calculations of CD Si supercells with revHC and WT functionals. All calculations are carried out with the OE-SCF solver [43].

[1] P. Hohenberg and W. Kohn, Phys. Rev. **136**, B864 (1964).

[2] W. Kohn and L. J. Sham, Phys. Rev. **140**, A1133 (1965).

[3] S. Goedecker, Rev. Modern Phys. **71**, 1085 (1999).

[4] L. E. Ratcliff, S. Mohr, G. Huhs, T. Deutsch, M. Masella, and L. Genovese, Wiley Interdiscip. Rev.: Comput. Mol. Sci. **7**, e1290 (2017).

[5] W. C. Witt, B. G. Del Rio, J. M. Dieterich, and E. A. Carter, J. Mater. Res. **33**, 777 (2018).

[6] V. V. Karasiev and S. B. Trickey, Comput. Phys. Commun. **183**, 2519 (2012).

[7] W. Mi, X. Shao, C. Su, Y. Zhou, S. Zhang, Q. Li, H. Wang, L. Zhang, M. Miao, Y. Wang, and Y. Ma, Comput. Phys. Commun. **200**, 87 (2016).

[8] P. Cortona, Phys. Rev. B **44**, 8454 (1991).

[9] T. A. Wesolowski and A. Warshel, J. Phys. Chem. **97**, 8050 (1993).

[10] A. Krishtal, D. Sinha, A. Genova, and M. Pavanello, J. Phys.: Condens. Matter **27**, 183202 (2015).

[11] W. Mi and M. Pavanello, J. Phys. Chem. Lett. **11**, 272 (2020).

[12] X. Shao, Q. Xu, S. Wang, J. Lv, Y. Wang, and Y. Ma, Comput. Phys. Commun. **233**, 78 (2018).

[13] L. Hung and E. A. Carter, Chem. Phys. Lett. **475**, 163 (2009).

[14] X. Shao, K. Jiang, W. Mi, A. Genova, and M. Pavanello, Wiley Interdiscip. Rev.: Comput. Mol. Sci. **11**, e1482 (2021).

[15] L. H. Thomas, Math. Proc. Cambridge Philos. Soc. **23**, 542 (1927).

[16] E. Fermi, Rend. Accad. Naz. Lincei **6**, 602 (1927).

[17] D. García-Aldea and J. Alvarellos, J. Chem. Phys. **127**, 144109 (2007).

[18] A. J. Thakkar, Phys. Rev. A **46**, 6920 (1992).

[19] L.-W. Wang and M. P. Teter, Phys. Rev. B **45**, 13196 (1992).

[20] E. Smargiassi and P. A. Madden, Phys. Rev. B **49**, 5220 (1994).

[21] F. Perrot, J. Phys.: Condens. Matter **6**, 431 (1994).

[22] Y. A. Wang, N. Govind, and E. A. Carter, Phys. Rev. B **58**, 13465 (1998).

[23] W. Mi, A. Genova, and M. Pavanello, J. Chem. Phys. **148**, 184107 (2018).

[24] Q. Xu, Y. Wang, and Y. Ma, Phys. Rev. B **100**, 205132 (2019).

[25] E. Chacón, J. E. Alvarellos, and P. Tarazona, Phys. Rev. B **32**, 7868 (1985).

[26] P. García-González, J. E. Alvarellos, and E. Chacón, Phys. Rev. A **54**, 1897 (1996).

[27] Y. A. Wang, N. Govind, and E. A. Carter, Phys. Rev. B **60**, 16350 (1999).

[28] C. Huang and E. A. Carter, Phys. Rev. B **81**, 045206 (2010).

[29] W. Mi and M. Pavanello, Phys. Rev. B **100**, 041105(R) (2019).

[30] Q. Xu, J. Lv, Y. Wang, and Y. Ma, Phys. Rev. B **101**, 045110 (2020).

[31] J. P. Perdew and L. A. Constantin, Phys. Rev. B **75**, 155109 (2007).

[32] S. Laricchia, L. A. Constantin, E. Fabiano, and F. Della Sala, J. Chem. Theory Comput. **10**, 164 (2014).

[33] S. Śmiga, E. Fabiano, L. A. Constantin, and F. Della Sala, J. Chem. Phys. **146**, 064105 (2017).

[34] L. A. Constantin, E. Fabiano, and F. Della Sala, J. Phys. Chem. Lett. **9**, 4385 (2018).

[35] K. Luo, V. V. Karasiev, and S. B. Trickey, Phys. Rev. B **98**, 041111(R) (2018).

[36] F. Sarcinella, E. Fabiano, L. A. Constantin, and F. Della Sala, Phys. Rev. B **103**, 155127 (2021).

[37] J. Xia, C. Huang, I. Shin, and E. A. Carter, J. Chem. Phys. **136**, 084102 (2012).

[38] I. Shin and E. A. Carter, J. Chem. Phys. **140**, 18A531 (2014).

[39] R. M. Pick, M. H. Cohen, and R. M. Martin, Phys. Rev. B **1**, 910 (1970).

[40] M. Levy and J. P. Perdew, Phys. Rev. A **32**, 2010 (1985).

[41] G. K.-L. Chan and N. C. Handy, Phys. Rev. A **59**, 3075 (1999).

[42] E. H. Lieb and S. Oxford, Int. J. Quantum Chem. **19**, 427 (1981).

[43] X. Shao, W. Mi, and M. Pavanello, J. Phys. Chem. Lett. **12**, 4134 (2021).

[44] C. v. Weizsäcker, Z. Phys. **96**, 431 (1935).

[45] O. A. Vydrov and T. Van Voorhis, J. Chem. Phys. **133**, 244103.

[46] K. Lee, É. D. Murray, L. Kong, B. I. Lundqvist, and D. C. Langreth, Phys. Rev. B **82**, 081101(R) (2010).

[47] G. Román-Pérez and J. M. Soler, Phys. Rev. Lett. **103**, 096102.

[48] DFTPY, dftpy.rutgers.edu.

[49] S. J. Clark, M. D. Segall, C. J. Pickard, P. J. Hasnip, M. J. Probert, K. Refson, and M. Payne, Z. Kristallogr. **220**, 567 (2005).

[50] C. Huang and E. A. Carter, Phys. Chem. Chem. Phys. **10**, 7109 (2008).

[51] W. Mi, S. Zhang, Y. Wang, Y. Ma, and M. Miao, J. Chem. Phys. **144**, 134108 (2016).

[52] J. P. Perdew and A. Zunger, Phys. Rev. B **23**, 5048 (1981).

[53] F. Murnaghan, Proc. Natl. Acad. Sci. USA **30**, 244 (1944).

[54] A. H. Larsen, J. J. Mortensen, J. Blomqvist, I. E. Castelli, R. Christensen, M. Dułak, J. Friis, M. N. Groves, B. Hammer, C. Hargus, E. D. Hermes, P. C. Jennings, P. B. Jensen, J. Kermode, J. R. Kitchin, E. L. Kolsbjerg, J. Kubal, K. Kaasbjerg, S. Lysgaard, J. B. Maronsson, T. Maxson, T. Olsen, L. Pastewka, A. Peterson, C. Rostgaard, J. Schiøtz, O. Schütt, M. Strange, K. S. Thygesen, T. Vegge, L. Vilhelmsen, M. Walter, Z. Zeng, and K. W. Jacobsen, J. Phys.: Condens. Matter **29**, 273002 (2017).

[55] *Semiconductors: Basic Data*, edited by O. Madelung (Springer, Berlin, 1996).

[56] M. Chen, J. Xia, C. Huang, J. M. Dieterich, L. Hung, I. Shin, and E. A. Carter, Comput. Phys. Commun. **190**, 228 (2015).

[57] G. S. Ho, V. L. Lignères, and E. A. Carter, Comput. Phys. Commun. **179**, 839 (2008).

[58] See Supplemental Material at http://link.aps.org/supplemental/10.1103/PhysRevB.104.045118 for additional tables and figures.

[59] K. F. Garrity, J. W. Bennett, K. M. Rabe, and D. Vanderbilt, Comput. Mater. Sci. **81**, 446 (2014).

[60] R. Tran, Z. Xu, B. Radhakrishnan, D. Winston, W. Sun, K. A. Persson, and S. P. Ong, Sci. Data **3**, 160080 (2016).

[61] R. Jaccodine, J. Electrochem. Soc. **110**, 524 (1963).

[62] D. J. Eaglesham, A. E. White, L. C. Feldman, N. Moriya, and D. C. Jacobson, Phys. Rev. Lett. **70**, 1643 (1993).

[63] C. Messmer and J. Bilello, J. Appl. Phys. **52**, 4623 (1981).

[64] X. Shao, W. Mi, Q. Xu, Y. Wang, and Y. Ma, J. Chem. Phys. **145**, 184110 (2016).